Ordered Mesoporous Sb-, Nb-, and Ta-Doped SnO_2 Thin Films with Adjustable Doping Levels and High Electrical Conductivity

Yude Wang,[†,*] Torsten Brezesinski,[‡] Markus Antonietti,[†] and Bernd Smarsly[†,‡]

[†]Max Planck Institute of Colloids and Interfaces, Research Campus Golm, 14476 Potsdam, Germany, and [‡]Institute of Physical Chemistry, Justus-Liebig-University Giessen, 35392 Giessen, Germany

ABSTRACT This paper describes the synthesis and electrical properties of self-organized Sb-, Nb-, and Ta-doped SnO_2 thin films with adjustable doping levels. These transparent conducting oxides (TCOs) were prepared using a poly(ethylene-*co*-butylene)-*b*-poly(ethylene oxide) diblock copolymer as well as a novel polyisobutylene-*b*-poly(ethylene oxide) as organic templates. All samples are highly crystalline and have ordered cubic pore-solid architectures after removal of the polymer template by calcination; however, the electrical conductivity is not identical. The films are characterized by a combination of small- and wide-angle X-ray diffraction/scattering, SEM/TEM imaging, and X-ray photoelectron spectroscopy. Resistivity measurements conducted on the mesoporous frameworks show that the electrical properties strongly depend on both the degree of crystallinity and the elemental makeup. Considerable enhancements of the electrical properties result when the films are doped with antimony and treated in N_2 at elevated temperatures. Such TCO materials show electrical resistivities which are—despite the mesoporous morphology—only 1 order of magnitude higher than reported values for dense Sb-doped SnO_2 films.

KEYWORDS: transparent conducting oxides · mesoporous · thin films · sol–gel · nanomaterials

Tin oxide (SnO_2) is a semiconductor with a band gap of 3.62 eV at 298 K and is particularly interesting because of its low electrical resistance associated with high transparency in the UV–visible region.[1,2] In recent years, it has been shown that for SnO_2 and other semiconducting oxides, such as ZnO or In_2O_3, the charge carrier concentration and, thus, the electrical conductivity can be strongly increased by extrinsic dopants.[3–5] In the case of tin oxide, antimony (Sb), niobium (Nb), and tantalum (Ta) are most commonly used as doping agents (donor materials) to achieve high n-type conductivity while maintaining high optical transparency.[6,7] In recent years, these doped tin oxides have been explored as potential replacement of indium tin oxide (ITO) due to shortage of indium.

Transparent conducting oxides (TCOs) play an integral role in optoelectronic, electrochromic, and electroluminescent devices.[8–10] In particular, advancements that receive widespread attention are those that allow for control of the electrical conductivity or nanoscale architectures which lend themselves to hybrid structures with a desirable combination of properties that are not easily achieved by other means. We believe that TCOs with periodic pore architectures in the nanorange and high interface areas can be a device platform which offers such advances. It has, for example, already been shown that mesoporous TCO films allow the incorporation of electrochemically active species.[5] Furthermore, it should be possible to electrochemically deposit a wide variety of materials, including metals, alloys, and metal oxides into the framework, which would automatically lead to the formation of zero-dimensional nanostructures with the pores. Also, the large surface areas of these materials allow the chemical linkage of significant amounts of redox-active enzymes to the inorganic pore walls, which may be useful for the development of novel sensors. The incorporation of dyes and semiconductors, by contrast, offers the opportunity to design alternative types of solar cells. Compared to more standard solar cells made of nanostructured metal oxides modified with sensitizing dye, a device made from mesoporous TCOs would facilitate the electron transport properties. Overall, transparent conducting oxides in the form of thin films can be used for a broad range of applications, but to date, only mesoporous ITO has been reported.[5]

Polymer and surfactant templating provides a unique, simple method for producing ordered porous inorganic materials with

*Address correspondence to yude.wang@mpikg.mpg.de.

Received for review February 3, 2009 and accepted April 24, 2009.

Published online May 12, 2009.
10.1021/nn900108x CCC: $40.75

© 2009 American Chemical Society

precisely defined nanoscale architectures. Such materials can be readily formed as either bulk powders or thin films by solution phase co-assembly of inorganic oligomers with amphiphilic surfactants or block copolymers.[11,12] Much of the thin film work makes use of evaporation-induced self-assembly (EISA) to generate homogeneous composite films on virtually any substrate.[13,14] These composites are then made porous by removing the organic template to leave only the cross-linked inorganic framework. However, the majority of the self-organized film materials prepared in this manner do not possess the potential for crystalline grains while retaining nanoscale order. The reason for this can be attributed to the lack of control over crystallization. Thus, to the best of our knowledge, there is no report on conductive SnO_2-based systems with nanoscale periodicity.

In this work, we show that mesoporous TCOs can be produced that still possess fully crystalline frameworks by moving to a templated structure with sufficiently thick pore walls.[19,21] It is therefore crucial that the micelles formed are sufficiently large to allow for thick pore walls needed to host nanometer-sized crystals of the respective oxide. Since the thickness of the inorganic wall between two adjacent micelles is determined by their size, at least 15−20 nm diameter micelles are needed to ensure that mesoscale order is retained after crystallization of the initially amorphous framework.[19,21] Instead of using structure-directing agents (SDAs) of the Pluronic family, which have been shown to produce mesostructured films with 4−6 nm thick pore walls (in most cases, the nanoscale structure is not well-preserved after crystallization),[15−17] we used one of the large poly(ethylene-*co*-butylene)-*b*-poly(ethylene oxide) diblock copolymers (also referred to as KLE)[18] as well as a novel polyisobutylene-*b*-poly(ethylene oxide). Both templates form ordered cubic pore-solid architectures with 25−35 nm pore-to-pore distances and 10−15 nm thick pore walls. Recent work has clearly shown that SDAs of the KLE family possess many desirable templating properties, including high thermal stability and a strong tendency to form ordered structures in a broad range of solvents (strong segregation strength, low alcohol sensitivity, *etc.*). Unlike Pluronic templates, these block copolymers are well-suited for the preparation of large-pore metal oxide thin films with nanoscale periodicity and fully crystalline framework.[19−21]

In this paper, we examine the preparation of periodic mesoporous Sb-, Nb-, and Ta-doped SnO_2 thin films and explore the electrical properties as a function of doping level and crystallinity of the wall structure using a four-probe technique. Through these experiments, interplay between crystallinity, elemental makeup, and conductivity is probed.

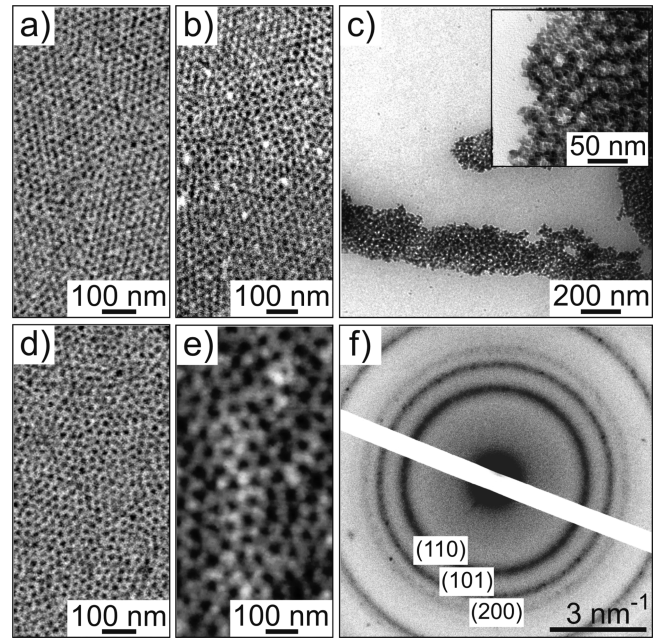

Figure 1. (a,b) Top-view FESEM images of KLE22-templated NTO-11 and TTO-10 thin films, showing open pores at the solid−air interface. (c−f) Nanoscale structure of PIB6000-templated ATO-15 thin films. (c) Low-magnification bright-field TEM image, showing the periodic nature of the porosity. Inset: higher magnification TEM image. (d) Top-view FESEM image. (e) Tapping mode AFM image. (f) SAED pattern of a region similar to that shown in (c). All samples had been treated at 550 °C for 1 min in air.

RESULTS AND DISCUSSION

The nanoporous TCO films employed in this work were synthesized using an evaporation-induced self-assembly process as mentioned above. Briefly, an ethanolic solution containing a tin oxide precursor and dopant as well as an organic template is dip-coated onto a polar substrate. Upon evaporation, the system co-assembles to form an inorganic/organic composite with nanoscale periodicity. This composite is then thermally treated to remove the organic template and to crystallize the initially amorphous pore walls. Besides the KLE22 diblock copolymer,[18] which has frequently been used to produce thermally stable and highly crystalline metal oxide frameworks with uniform spherical pores,[19−21] we also used a novel polyisobutylene-*b*-poly(ethylene oxide) (referred to as PIB6000). Interestingly, this porogen shows comparable templating properties to KLE22 and is thus also highly suitable for synthesizing thin film materials. In the following, ATO refers to antimony-doped tin oxide, while NTO and TTO refer to niobium- and tantalum-doped SnO_2, respectively. The number following the three letter code represents the doping level according to the recipe used.

Figure 1a,b presents top-view field-emission scanning electron microscope (FESEM) images of KLE22-templated NTO-11 and TTO-10 thin films that have been subjected to an annealing temperature of 550 °C.

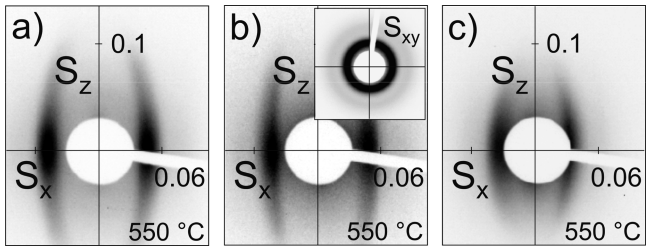

Figure 2. Two-dimensional SAXS patterns for KLE22-templated NTO-11 (a) and TTO-10 (b) as well as for PIB6000-templated ATO-15 (c). The patterns were taken in reflection (angle of incidence $\beta = 5°$) and transmission mode ($\beta = 90°$, inset in b) and show characteristic reflections for bcc mesophases. Scattering vector *s* components are given in units of 1/nm; $s = 2/\lambda \sin\theta$.

Both show ordered cubic pore-solid architectures with 13−14 nm diameter pores and underline the macroscopic homogeneity. The high-quality lattices are characteristic of metal oxide films produced with the diblock copolymer KLE22. Figure 1 further shows an FESEM image of a PIB6000-templated ATO-15 thin film. Both the structure of the porosity and the 15−17 nm diameter pores are slightly lower quality compared to the KLE22-templated films. This corresponds well with TEM data (Figure 1c and Supporting Information Figure S1), showing a homogeneous distribution of somewhat deformed mesopores. Overall, FESEM clearly demonstrates that both KLE22- and PIB6000-templated films are crack-free and, more importantly, that the pores at the air−solid interface are open.

The macroscopic homogeneity is also observed with tapping mode atomic force microscopy (AFM). Figure 1e shows an AFM image of an ATO-15 thin film, which emphasizes the flatness of the top surface with a root-mean-square roughness of less than 2 nm. According to electron diffraction (Figure 1f), all films are highly crystalline with randomly oriented grains. Lattice spacings calculated from the diffraction rings are in perfect agreement with tetragonal tin stone (synthetic cassiterite). Taking into account the results from imaging, these data suggest that mesoporous SnO_2-based systems are very robust at overcoming stress that builds into the material over the course of thermal treatment, particularly during crystallization.

These results are further supported by two-dimensional small-angle X-ray scattering (2D-SAXS) data collected on a laboratory rotating anode. Films on ultrathin silicon substrates allowed the measurements to be performed at arbitrary angles of incidence β in order to monitor the structural evolution in and out of the plane of the films upon heating. Figure 2 shows 2D-SAXS patterns for PIB6000-templated ATO-15 as well as for KLE22-templated NTO-11 and TTO-10 taken after calcination at 550 °C in air. For small angles of incidence, the KLE22-templated films produce patterns with distinct in-plane scattering maxima. These maxima can be indexed in terms of a body-centered cubic (bcc) pore structure with (110) orientation relative to the plane of the substrate (often observed for metal oxide phases produced with KLE diblock copolymers).[20−22] PIB6000-templated films, by contrast, produce less defined but still clear in-plane scattering maxima. This is characteristic of a cubic pore-solid architecture possessing a higher degree of lattice distortions. Also, it is observed that the in-plane lattice parameter is larger by about 30% compared to KLE22-templated TCOs, which corroborates the observations made from SEM/TEM.

The 2D-SAXS experiments were also conducted on samples that had been heated to lower annealing temperatures (Supporting Information Figure S2). The reason for this is the fact that patterns obtained from amorphous films allow decisive clarification of the structure of the porosity, as the samples exhibit a much lower degree of lattice distortions/contraction. These 2D-SAXS data show a strong off-specular reflection for KLE-templated TCO films, the position of which is characteristic of a bcc mesostructure with (110) orientation.[23] The square arrangement of pores in the top layer suggests the presence of domains with (100) orientation relative to the plane of the substrate. Nonetheless, it should be taken into account that the orientation of pores at the air−solid interface can be different from that in the bulk.

In both cases, the materials calcined at 550 °C seem to have lost the out-of-plane periodicity of the mesostructure. This, however, can be explained by the film dimensions and the fact that the crystallization of the initially amorphous pore walls is always accompanied by the appearance of lattice distortions. The patterns further indicate anisotropic lattice contraction. A volume change of more than 55% is determined perpendicular to the plane of the substrate for both KLE22- and PIB6000-templated TCOs. The 2D-SAXS patterns taken in transmission mode (*i.e.*, $\beta = 90°$) show isotropic diffraction rings (shown for TTO-10 in Figure 2b), which suggest the presence of polycrystalline domains parallel to the substrate (see Figure 1a,b), and confirm the high degree of in-plane ordering. Moreover, 2D-SAXS clearly demonstrates that both cubic pore-solid architectures can be retained up to about 650 °C.

Note that electron microscopy just as small-angle X-ray scattering does not provide insight into the accessibility of pores. In our previous work on KLE-templated sol−gel-type SnO_2, however, ellipsometry porosimetry measurements revealed that the vast majority of the mesopores is accessible and that both pore size and Brunauer−Emmett−Teller surface area correspond well with results for other materials produced using the same templates.[21,22]

To verify the crystallization of the pore wall structure and to track the nanocrystal growth, temperature-dependent wide-angle X-ray diffraction (WAXD) mea-

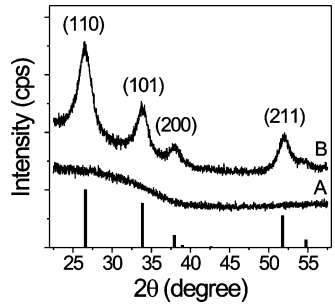

Figure 3. WAXD patterns of self-organized ATO-15 films heated to annealing temperatures of 300 °C (A) and 650 °C (B). The line pattern shows reference card #41-1445 for tetragonal tin stone according to JCPDS.

surements were conducted (Figure 3). These experiments show the different mesoporous TCO frameworks to be composed of randomly oriented cassiterite grains (shown for ATO-15 in Figure 2) as corroborated with JCPDS reference card #41-1445. The crystallization begins at around 400 °C, leading to rather small nanocrystals with an average size of 2−3 nm. This is in agreement with undoped mesoporous SnO_2 films.[22] It is observed that the full width at half-maximum intensity of the peaks slowly decreases with increasing temperature, which indicates a gradual nanocrystal growth in the pore walls accompanied by an increase in the degree of crystallinity. The average grain sizes were calculated, using the Scherrer equation, to range from 2−3 nm at 400 °C to 7−8 nm at 650 °C. Annealing temperatures of more than 650 °C, however, result in a rapid increase in grain size associated with the loss of nanoscale order. Also, note that irrespective of doping level, no phase change occurs and, more importantly, that no nanoscale phase separation is observed. This implies a homogeneous distribution of dopant ions in the SnO_2 lattice (rather than a mixture of the respective oxides). Similar results were obtained for NTO and TTO frameworks (Supporting Information Figure S3).

To determine the elemental makeup as well as the oxidation state of antimony, X-ray photoelectron spectroscopy (XPS) measurements were conducted on the mesoporous ATO thin films. Survey scans (Supporting Information Figure S3) were taken for all of the samples and verify the absence of any contaminants. Besides a weak C1s, which can be unambiguously attributed to hydrocarbons adsorbed onto the film surface, only tin, antimony, and oxygen-related core levels are observed. Figure 4a presents a comparison of the Sn3d level for films with various compositions ranging from weakly to highly doped SnO_2. The spectra show two symmetric peaks due to spin−orbit splitting with binding energies of 495.15 ± 0.05 and 486.7 ± 0.05 eV for the $d_{3/2}$ and $d_{5/2}$ lines, respectively. Both peak position and separation (8.4 eV) correspond well with reference data.[24,25] Figure 4b compares the Sb3d and O1s levels for the same samples. One can clearly see that the peak

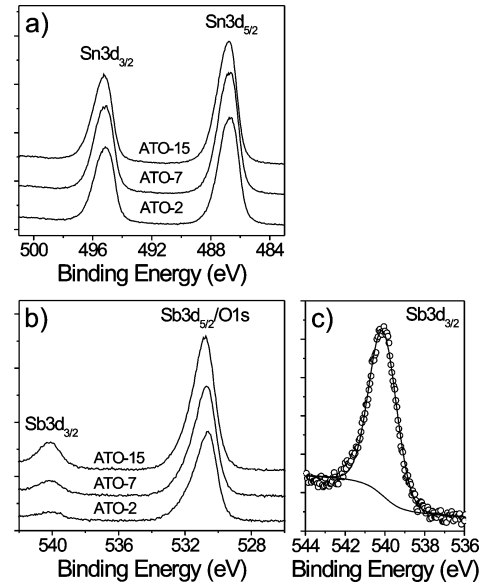

Figure 4. High-resolution XPS spectra for PIB6000-templated ATO thin films with different doping levels. (a) Scans of the Sn3d region. (b) Scans of the Sb3d and O1s regions. (c) Spectrum of the $Sb3d_{3/2}$ peak for an ATO-15 film and corresponding fit data. All samples had been treated at 550 °C for 1 min in air.

intensity of the $Sb3d_{3/2}$ line increases with increasing Sb content. The binding energies were determined to be 540.1 ± 0.05 eV for $Sb3d_{3/2}$, 531.8 ± 0.05 eV for $Sb3d_{5/2}$, and 530.8 ± 0.05 eV for O1s. Note that the peaks for the latter two are superimposed. Elemental analyses carried out by comparing the area of the Sn3d and Sb3d peaks and then taking into account for the sensitivity factors yield Sb concentrations of 1.76 mol % for ATO-2, 6.01 mol % for ATO-7, and 12.87 mol % for ATO-15. We assume that the sensitivity of $Sb(OC_2H_5)_3$ toward water leads to the slight loss of antimony.[26]

According to Terrier *et al.*, the peak position of the $Sb3d_{3/2}$ line can be used to distinguish between Sb^{3+} and Sb^{5+}.[26,27] Figure 4c shows a highly symmetric peak for mesoporous ATO-15, indicating one single oxidation state which is identified as Sb^{5+} from the binding energy of 540.15 eV. This result is in good agreement with previously reported near-edge X-ray absorption fine structure (XANES) data, suggesting that the largest fraction of antimony is already in the highest oxidation state after heating ATO films to 100 °C.[28] We thus assume that the antimony species with lower valence state get oxidized over the course of thermal treatment. Overall, XPS confirms the formation of chemically pure, n-type ATO thin films.

Resistivity measurements were conducted on the mesoporous frameworks to learn about the interplay between crystallinity, chemical composition, and electrical conductivity (Table 1). Figure 5 shows the specific resistivity as a function of doping level for films that were heated to different annealing temperatures in air. The graph illustrates a clear change in resistivity with doping concentration, which can be attributed to the

TABLE 1. Specific Resistivity of Cubic Mesoporous ATO Thin Films

doping level[a] (mol %)	450 °C in air[b] (Ω · cm)	treated in N_2[c] (Ω · cm)	550 °C in air[b] (Ω · cm)	treated in N_2[c] (Ω · cm)	650 °C in air[b] (Ω · cm)	treated in N_2[c] (Ω · cm)
0.0	3.36×10^{2}	3.14×10^{0}	4.44×10^{1}	2.51×10^{0}	1.50×10^{2}	3.66×10^{-1}
2.5	1.15×10^{0}	2.18×10^{-1}	2.42×10^{-1}	9.56×10^{-2}	1.76×10^{-1}	9.34×10^{-2}
5.0	3.38×10^{-1}	7.48×10^{-2}	8.86×10^{-2}	4.92×10^{-2}		
7.5	5.36×10^{-1}	8.82×10^{-2}	1.34×10^{-1}	6.04×10^{-2}	5.74×10^{-2}	3.70×10^{-2}
10.0	3.44×10^{-1}	7.98×10^{-2}	8.96×10^{-2}	4.22×10^{-2}		
15.0	4.78×10^{-1}	1.12×10^{-1}	7.70×10^{-2}	3.98×10^{-2}	4.90×10^{-2}	3.44×10^{-2}

[a]Antimony doping level according to the recipe used. [b]Thermally treated at 450, 550, and 650 °C for 1 min. [c]Thermally treated at 450 °C for 30 min.

increase in the number of free charge carriers. The change in resistivity is not linear but follows a trend often observed for ATO.[27,29] The least specific resistivity, obtained for mesoporous ATO-15 calcined at 650 °C in air (4.90×10^{-2} Ω · cm), is only 1 order of magnitude higher than reported values for dense ATO films (4×10^{-3} Ω · cm).[30−32] Moreover, after treating the films in a reducing atmosphere at 450 °C, the film resistivity drops

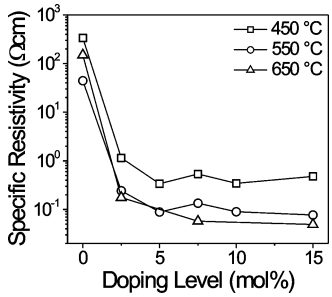

Figure 5. Specific resistivity as a function of doping level for PIB6000-templated ATO films. The mesoporous samples had been treated at 450, 550, and 650 °C for 1 min in air.

(4.90×10^{-2} *vs* 3.44×10^{-2} Ω · cm) due to the increase in the concentration of free charge carriers through the formation of oxygen vacancies. The resultant specific resistivities are quite low when taking into account the mesoporous morphology (lower conducting mass and conduction pathways) and are only about 1 order of magnitude higher compared to bulk ATO films. Similar results were obtained for KLE22-templated NTO and TTO films (Supporting Information Table S1).

CONCLUSIONS

In this work, mesoporous ATO was obtained starting from molecular precursors and taking advantage of the superior templating properties of KLE22 and PIB6000. The mesoporosity was shown to be retained during thermal treatment needed to form the crystalline oxide. As expected for nanoscale TCO materials, the conductivity does not reach the values found for commercial ITO and ATO films, respectively. This drawback, however, is compensated by the fact that the presence of porosity can be used for novel applications. The porosity offers the opportunity to combine the low electrical resistance and high transparency in the UV−visible region with electrochemically active moieties (such as electrolytes and conjugated polymers) and so forth. For instance, Guo *et al.* observed a very fast electron transfer between ATO and certain poly(phenylene vinylene) polymers.[33] Such properties could be interesting for electro-optical applications *etc.* Moreover, Marcel *et al.* described promising electrochromic properties of ATO films.[34] In all of these applications, the presence of mesoporosity would be helpful to enhance the interaction with guest molecules. Overall, the design parameters described here provide a blueprint for future TCO materials, which lend themselves to hybrid structures.

EXPERIMENTAL SECTION

Materials. $SnCl_4$ (99.9%), $Sb(OC_2H_5)_3$ (99.9%), $Nb(OC_2H_5)_5$ (99.9%), and $Ta(OC_2H_5)_5$ (99.9%) were purchased from Sigma-Aldrich. $H(CH_2CH_2CH_2(CH)CH_2CH_3)_{89}(OCH_2CH_2)_{79}OH$ (referred to as KLE22) was synthesized in our laboratories,[18] and $CH_3C(CH_3)_2(CH_2C(CH_3)_2)_{107}CH_2C(CH_3)_2C_6H_4O(CH_2CH_2O)_{100}H$ (referred to as PIB6000) was obtained from BASF.

Synthesis. In a water-free container, both $SnCl_4$ and dopant are carefully combined with dry EtOH. Once the solution is homogeneous, either PIB6000 or KLE22 (30 wt % with respect to the amount of tin oxide formed) dissolved in EtOH/THF (1:1) is added. After 24 h of stirring, thin films are produced *via* dip-coating on polar substrates. Optimal conditions include 15−18% relative humidity and a constant withdrawal rate of 10 mm/s. The films need to be aged at 200 °C for 12 h prior to template removal to prevent loss of nanoscale order over the course of crystallization. For best results, films are calcined using a 1 h ramp to 600 °C in air followed by a 1 min soak. To improve the electrical conductivity, the samples are treated at 450−500 °C in nitrogen for 30 min.

Methods. TEM images were taken with a Zeiss EM 912Ω at an acceleration voltage of 120 kV. Tapping mode AFM images were collected on a multimode AFM from Vecco Instruments employing Olympus microcantilevers (resonance frequency = 300 kHz, force constant = 42 N/m). FESEM images were taken with a LEO440 instrument equipped with an InLens detector (acceleration voltage = 2.0 kV).

WAXD measurements were carried out on a D8 diffractometer from Bruker instruments (Cu Kα radiation) equipped with an energy dispersive solid-state detector. The 2D-SAXS patterns were collected on a Nonius rotating anode with pinhole collimation and MAR CCD area detector (sample−detector distance = 750 mm). The use of ultrathin silicon wafers (*ca.* 30 μm) as substrates allowed these measurements to be performed at various angles of incidence β (defined as the angle between the X-ray beam and the plane of the substrate). XPS spectra were acquired on an ESCALAB 250 spectrometer with monochromatic Al Kα X-ray source (power = 250 W). The electron takeoff angle to the sample surface was adjusted to 45°. The adventitious hydrocar-

bon C1s signal at 284.6 eV was used as the energy reference to correct for charging. Resistivity measurements were conducted using a four-probe technique (Keithley Instruments, Model 2000) to eliminate the effects of contact resistances. The specific resistivity ρ was calculated from the measured resistance R as follows: $\rho = R\pi t/\ln 2$, in which t represents the film thickness.

Acknowledgment. The authors thank A. Heilig and R. Pitschke for their contributions. This work was supported by the Max-Planck-Society and the German Research Society. Y.W. acknowledges the support of an Alexander von Humboldt fellowship.

Supporting Information Available: Additonal figures and table. This material is available free of charge *via* the Internet at http://pubs.acs.org.

REFERENCES AND NOTES

1. Batzill, M.; Diebold, U. The Surface and Materials Science of Tin Oxide. *Prog. Surf. Sci.* **2005**, *79*, 47–154.
2. Amma, D. S. D.; Vaidyan, V. K.; Manoj, P. K. Structural, Electrical and Optical Studies on Chemically Deposited Tin Oxide Films from Inorganic Precursors. *Mater. Chem. Phys.* **2005**, *93*, 194–201.
3. Dawar, A. L.; Joshi, J. C. Semiconducting Transparent Thin Films: Their Properties and Applications. *J. Mater. Sci.* **1984**, *19*, 1–23.
4. Singh, A. V.; Mehra, R. M.; Yoshida, A.; Wakahara, A. Doping Mechanism in Aluminum Doped Zinc Oxide Films. *Appl. Phys. Lett.* **2004**, *95*, 3640–3643.
5. Fattakhova Rohlfing, D.; Brezesinski, T.; Rathouský, J.; Feldhoff, A.; Oekermann, T.; Wark, M.; Smarsly, B. Transparent Conducting Films of Indium Tin Oxide with 3D Mesopore Architecture. *Adv. Mater.* **2006**, *18*, 2980–2983.
6. Lee, S. W.; Kim, Y. W.; Chen, H. D. Electrical Properties of Ta-Doped SnO_2 Thin Films Prepared by the Metal-Organic Chemical-Vapor Deposition Method. *Appl. Phys. Lett.* **2001**, *78*, 350–352.
7. Dhage, S. R.; Ravi, V. Influence of Various Donors on Nonlinear I−V Characteristics of Tin Dioxide Ceramics. *Appl. Phys. Lett.* **2003**, *83*, 4539–4541.
8. Ju, S. Y.; Facchetti, A.; Xuan, Y.; Liu, J.; Ishikawa, F.; Ye, P. D.; Zhou, C. W.; Marks, T. J.; Janes, D. B. Fabrication of Fully Transparent Nanowire Transistors for Transparent and Flexible Electronics. *Nat. Nanotechnol.* **2007**, *2*, 378–384.
9. Hosono, H. Recent Progress in Transparent Oxide Semiconductors: Materials and Device Application. *Thin Solid Films* **2007**, *515*, 6000–6014.
10. Hao, X. T.; Tan, L. W.; Ong, K. S.; Zhu, F. R. High-Performance Low-Temperature Transparent Conducting Aluminum-Doped ZnO Thin Films and Applications. *J. Cryst. Growth* **2006**, *287*, 44–47.
11. Goltner, C. G.; Antonietti, M. Mesoporous Materials by Templating of Liquid Crystalline Phases. *Adv. Mater.* **1997**, *9*, 431–436.
12. Zhao, D. Y.; Feng, J. L.; Huo, Q. S.; Melosh, N.; Fredrickson, G. H.; Chmelka, B. F.; Stucky, G. D. Triblock Copolymer Syntheses of Mesoporous Silica with Periodic 50 to 300 Angstrom Pores. *Science* **1998**, *279*, 548–552.
13. Brinker, C. J.; Lu, Y. F.; Sellinger, A.; Fan, H. Y. Evaporation-Induced Self-Assembly: Nanostructures Made Easy. *Adv. Mater.* **1999**, *11*, 579–585.
14. Ogawa, M. Preparation of Layered Silica-Dialkyldimethylammonium Bromide Nanocomposites. *Langmuir* **1997**, *13*, 1853–1855.
15. Zhao, D.; Yang, P.; Melosh, N.; Feng, J.; Chmelka, B. F.; Stucky, G. D. Continuous Mesoporous Silica Films with Highly Ordered Large Pore Structures. *Adv. Mater.* **1998**, *10*, 1380–1385.
16. Richman, E.; Brezesinski, T.; Tolbert, S. H. Vertically Oriented Hexagonal Mesoporous Films Formed through Nanometre-Scale Epitaxy. *Nat. Mater.* **2008**, *7*, 712–717.
17. Alberius, P. C. A.; Frindell, K. L.; Hayward, R. C.; Kramer, E. J.; Stucky, G. D.; Chmelka, B. F. General Predictive Syntheses of Cubic, Hexagonal, and Lamellar Silica and Titania Mesostructured Thin Films. *Chem. Mater.* **2002**, *14*, 3284–3294.
18. Thomas, A.; Schlaad, H.; Smarsly, B.; Antonietti, M. Replication of Lyotropic Block Copolymer Mesophases into Porous Silica by Nanocasting: Learning about Finer Details of Polymer Self-Assembly. *Langmuir* **2003**, *19*, 4455–4459.
19. Brezesinski, T.; Groenewolt, M.; Gibaud, A.; Pinna, N.; Antonietti, M.; Smarsly, B. M. Evaporation-Induced Self-Assembly (EISA) at its Limit: Ultrathin, Crystalline Patterns by Templating of Micellar Monolayers. *Adv. Mater.* **2006**, *18*, 2260–2263.
20. Fattakhova-Rohlfing, D.; Wark, M.; Brezesinski, T.; Smarsly, B. M.; Rathousky, J. Highly Organized Mesoporous TiO_2 Films with Controlled Crystallinity—A Li-Insertion Study. *Adv. Funct. Mater.* **2007**, *17*, 123–132.
21. Brezesinski, T.; Wang, J.; Polleux, J.; Dunn, B.; Tolbert, S. H. Templated Nanocrystal-Based Porous TiO_2 Films for Next-Generation Electrochemical Capacitors. *J. Am. Chem. Soc.* **2009**, *131*, 1802–1809.
22. Brezesinski, T.; Fischer, A.; Iimura, K.; Sanchez, C.; Grosso, D.; Antonietti, M.; Smarsly, B. Generation of Self-Assembled 3D Mesostructured SnO_2 Thin Films with Highly Crystalline Frameworks. *Adv. Funct. Mater.* **2006**, *16*, 1433–1440.
23. Ruland, W.; Smarsly, B. M. Two-Dimensional Small-Angle X-ray Scattering of Self-Assembled Nanocomposite Films with Oriented Arrays of Spheres: Determination of Lattice Type, Preferred Orientation, Deformation and Imperfection. *J. Appl. Crystallogr.* **2007**, *40*, 409–417.
24. Montilla, F.; Morallon, E.; De Battisti, A.; Barison, S.; Daolio, S.; Vazquez, J. L. Preparation and Characterization of Antimony-Doped Tin Dioxide Electrodes. 3. XPS and SIMS Characterization. *J. Phys. Chem. B* **2004**, *108*, 15976–5981.
25. Liu, P. Y.; Chen, J. F.; Sun, W. D. Characterizations of SnO_2 and SnO_2:Sb Thin Films Prepared by PECVD. *Vacuum* **2004**, *76*, 7–11.
26. Terrier, C.; Chatelon, J. P.; Roger, J. A.; Berjoan, R.; Dubois, C. Analysis of Antimony Doping in Tin Oxide Thin Films Obtained by the Sol−Gel Method. *J. Sol−Gel Sci. Technol.* **1997**, *10*, 75–81.
27. Terrier, C.; Chatelon, J. P.; Berjoan, R.; Roger, J. A. Sb-Doped SnO_2 Transparent Conducting Oxide from the Sol−Gel Dip-Coating Technique. *Thin Solid Films* **1995**, *263*, 37–41.
28. Rockenberger, J.; zum Felde, U.; Tischer, M.; Troger, L.; Haase, M.; Weller, H. Near Edge X-ray Absorption Fine Structure Measurements (XANES) and Extended X-ray Absorption Fine Structure Measurements (EXAFS) of the Valence State and Coordination of Antimony in Doped Nanocrystalline SnO_2. *J. Chem. Phys.* **2000**, *112*, 4296–4304.
29. Zhang, D.; Deng, Z.; Zhang, J.; Chen, L. Microstructure and Electrical Properties of Antimony-Doped Tin Oxide Thin Film Deposited by Sol−Gel Process. *Mater. Chem. Phys.* **2006**, *98*, 353–357.
30. Minami, T. New n-Type Transparent Conducting Oxides. *MRS Bull.* **2000**, *25*, 38–44.
31. Goebbert, C.; Gasparro, G.; Schuler, T.; Krajewski, T.; Aegerter, M. A. Influence of the Layer Morphology on the Electrical Properties of Sol Gel Transparent Conducting Oxide Coatings. *J. Sol−Gel Sci. Technol.* **2000**, *19*, 435–439.
32. Nisiro, D.; Fabbri, G.; Celotti, G. C.; Bellosi, A. Influence of the Additives and Processing Conditions on the Characteristics of Dense SnO_2-Based Ceramics. *J. Mater. Sci.* **2003**, *38*, 2727–2742.
33. Guo, J. C.; She, C. X.; Lian, T. Q. Ultrafast Electron Transfer between Conjugated Polymer and Antimony-Doped Tin Oxide (ATO) Nanoparticles. *J. Phys. Chem. C* **2008**, *112*, 4761–4766.
34. Marcel, C.; Hegde, M. S.; Rougier, A.; Maugy, C.; Guery, C.; Tarascon, J. M. Electrochromic Properties of Antimony Tin Oxide (ATO) Thin Films Synthesized by Pulsed Laser Deposition. *Electrochim. Acta* **2001**, *46*, 2097–2104.